Accepted Manuscript

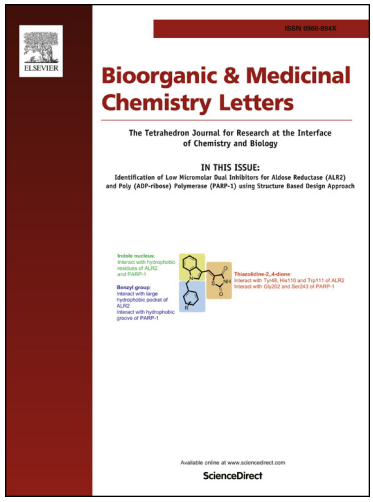

From a novel HTS hit to potent, selective, and orally bioavailable KDM5 inhibitors

Jun Liang, Sharada Labadie, Birong Zhang, Daniel F. Ortwine, Snahel Patel, Maia Vinogradova, James R. Kiefer, Till Mauer, Victor S. Gehling, Jean-Christophe Harmange, Richard Cummings, Tommy Lai, Jiangpeng Liao, Xiaoping Zheng, Yichin Liu, Amy Gustafson, Erica Van der Porten, Weifeng Mao, Bianca M. Liederer, Gauri Deshmukh, Le An, Yingqing Ran, Marie Classon, Patrick Trojer, Peter S. Dragovich, Lesley Murray

PII: S0960-894X(17)30491-2
DOI: http://dx.doi.org/10.1016/j.bmcl.2017.05.016
Reference: BMCL 24961

To appear in: *Bioorganic & Medicinal Chemistry Letters*

Received Date: 24 March 2017
Revised Date: 1 May 2017
Accepted Date: 3 May 2017

Please cite this article as: Liang, J., Labadie, S., Zhang, B., Ortwine, D.F., Patel, S., Vinogradova, M., Kiefer, J.R., Mauer, T., Gehling, V.S., Harmange, J-C., Cummings, R., Lai, T., Liao, J., Zheng, X., Liu, Y., Gustafson, A., Van der Porten, E., Mao, W., Liederer, B.M., Deshmukh, G., An, L., Ran, Y., Classon, M., Trojer, P., Dragovich, P.S., Murray, L., From a novel HTS hit to potent, selective, and orally bioavailable KDM5 inhibitors, *Bioorganic & Medicinal Chemistry Letters* (2017), doi: http://dx.doi.org/10.1016/j.bmcl.2017.05.016

From a novel HTS hit to potent, selective, and orally bioavailable KDM5 inhibitors

Jun Liang[a*], *Sharada Labadie*[a], *Birong Zhang*[a], *Daniel F. Ortwine*[a], *Snahel Patel*[a], *Maia Vinogradova*[a], *James R. Kiefer*[a], *Till Mauer*[a], *Victor S. Gehling*[b], *Jean-Christophe Harmange*[b], *Richard Cummings*[b], *Tommy Lai*[c], *Jiangpeng Liao*[c], *Xiaoping Zheng*[c], *Yichin Liu*[a], *Amy Gustafson*[a], *Erica Van der Porten*[a], *Weifeng Mao*[c], *Bianca M. Liederer*[a], *Gauri Deshmukh*[a], *Le An*[a], *Yingqing Ran*[a], *Marie Classon*[a], *Patrick Trojer*[b], *Peter S. Dragovich*[a], *Lesley Murray*[a]

a. Genentech Inc., 1 DNA Way, South San Francisco, California, 94080, USA
b. Constellation Pharmaceuticals Inc., 215 First Street, Suite 200, Cambridge, MA 02142, USA
c. WuXi AppTec Co., Ltd., 288 Fute Zhong Road, Waigaoqiao Free Trade Zone, Shanghai, 200131, China

AUTHOR EMAIL ADDRESS liang.jun@gene.com

RECEIVED DATE (to be automatically inserted after your manuscript is accepted)

CORRESPONDING AUTHOR FOOTNOTE *Corresponding Author. Tel: 650-467-3567, E-mail: liang.jun@gene.com

Table of contents graphic

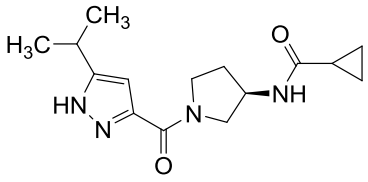

50

MW	290
LogD (pH 7.4)	1.3
KDM5A IC_{50}	45 nM
PC9 cell H3K4Me3 EC_{50}	960 nM
Mouse CLp	28 mL/min/kg
F	34%

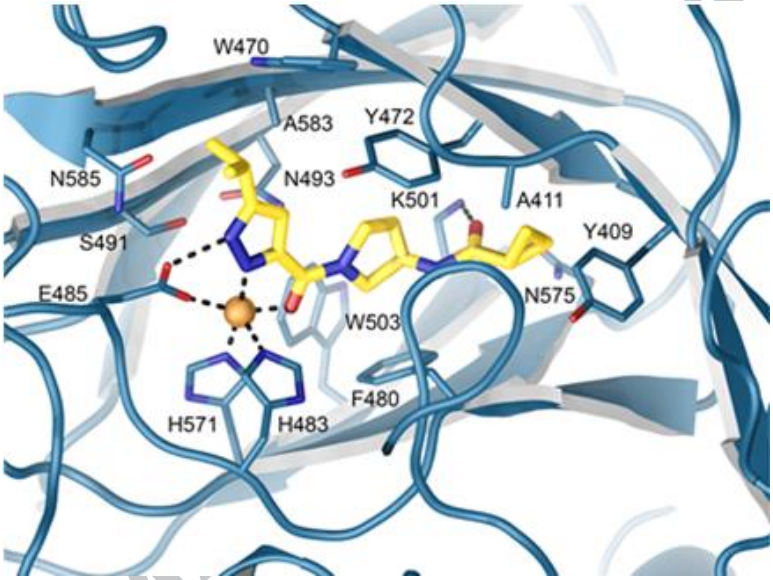

ABSTRACT: A high-throughput screening (HTS) of the Genentech/Roche library identified a novel, uncharged scaffold as a KDM5A inhibitor. Lacking insight into the binding mode, initial attempts to improve inhibitor potency failed to improve potency, and synthesis of analogs was further hampered by the presence of a C-C bond between the pyrrolidine and pyridine. Replacing this with a C-N bond significantly simplified synthesis, yielding pyrazole analog **35**, of which we obtained a co-crystal structure with KDM5A. Using structure-based design approach, we identified **50** with improved biochemical, cell potency and reduced MW and lower lipophilicity (LogD) compared with the original hit. Furthermore, **50** showed lower clearance than **9** in mice. In combination with its remarkably low plasma protein binding (PPB) in mice (40%), oral dosing of **50** at 5 mg/kg resulted in unbound C_{max} ~2-fold of its cell potency (PC9 H3K4Me3 0.96 μM), meeting our criteria for an *in vivo* tool compound from a new scaffold.

It is now widely accepted that DNA-histone interactions play an important role in modulating chromatin structure and, as a result, regulation of gene transcriptions.[1] An excellent example is the histone lysine acetyl modification, modulated by histone acetyltransferases (HATs) and histone deacetylases (HDACs), that have led to the discovery of several drugs approved for treating cancers.[2] More recently, histone lysine methylation states, which are determined by the interplay between histone methyltransferases and histone demethylases, have started to generate similar attention. The KDM5 family of histone demethylases (KDM5A-D) are Fe(II)- and 2-oxoglutarate (2-OG)-dependent oxygenases that specifically remove methyl groups from trimethylated lysine residues at the 4-position of histone 3 (H3K4Me3).[3] Disruption of KDM5 activity, either through RNAi or by a selective small molecule KDM5 inhibitor, reduced survival of drug-tolerant cancer cells *in vitro*.[4] Attracted by the therapeutic potential of reducing drug resistance in the clinic, several groups have recently disclosed small molecule KDM5 inhibitors[5] (**1-5, Figure 1**) as *in vitro* probes. We aimed to discover potent, selective, and orally bioavailable KDM5 inhibitors with excellent pharmacokinetics profiles in mice in order to further test the therapeutic hypothesis *in vivo*. Accordingly, we recently reported a promising [1,5-*a*]pyrimidin-7(4*H*)-one-containing lead molecule (**6**) that met our *in vivo* "tool compound" criteria.[6]

Despite the identification of **6**, we sought to identify a structurally and mechanistically distinct second scaffold to test our therapeutic hypothesis both *in vitro and in vivo*. And the rationales were two-fold. First, we reasoned that a structurally distinct scaffold might mitigate any potential safety liabilities associated with the [1,5-*a*]pyrimidin-7(4*H*)-one scaffold. Secondly, we noted that all the published KDM5 inhibitors (**1-6**) are weakly acidic and displayed a competitive mechanism of inhibition relative to co-substrate 2-OG. This is consistent with their

binding mode, as highlighted with a co-crystal structure of *N*-oxalylglycine (NOG) **1** with KDM5B (PDB code 5FV3),[5f] in which the distal carboxylic acid achieved strong ionic interactions with Lys501 in the active site. We sought to identify an uncharged inhibitor series, preferably competitive with histone substrate alone or in combination with 2-OG competition that might display smaller enzyme-cell potency shift in cells. Therefore, a HTS was conducted with the Genentech/Roche small molecule library, in search of additional structurally and mechanistically distinct hits against KDM5.

Figure 1.

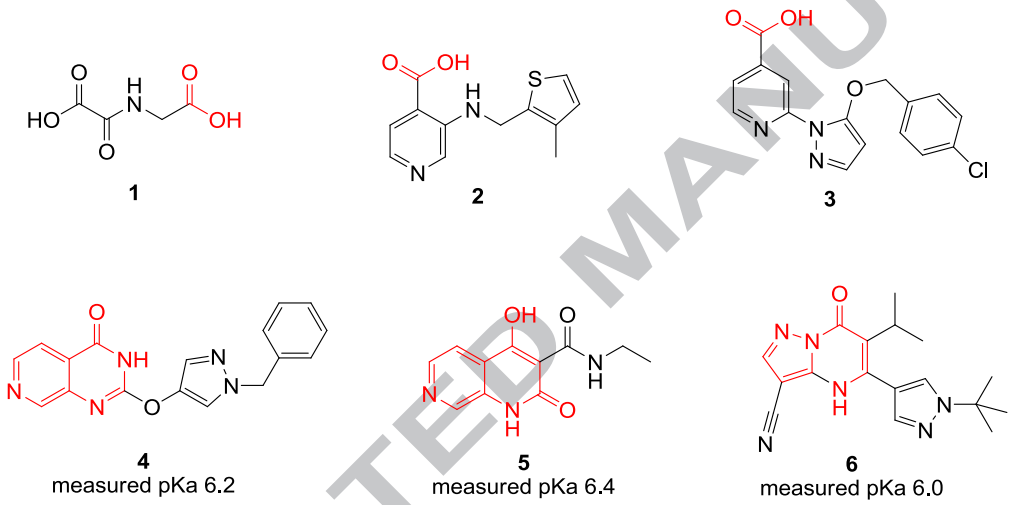

Figure 1. Reported KDM5 inhibitors and the measured pKa values.

From the HTS campaign, compound **7** (as a racemic mixture) emerged as an interesting hit with reasonable physiochemical properties (**Figure 2**) and excellent KDM5 potency (IC_{50} 0.26 μM, LE 0.33, LLE 4.0).[7] Additionally, **7** was found to be quite selective for KDM5, exhibiting IC_{50} > 25 μM against other KDMs (KDM1A, 2B, 3B, 4C, 6A and 7B were selected from each KDM family to assess a compound's KDM-selectivity. Only the IC_{50} values for KDM4C are shown in **Figure 2**, since it is closest to KDM5A by sequence and structure). More

importantly, the measured basic pKa for **7** was 6.1, a weak basic due to the pyridyl moiety. Therefore, **7** was expected to be mostly uncharged at physiological pH (7.4), in contrast to the majority of KDM5 inhibitors (**1-6**) reported in the literature which were weakly acidic and negatively charged. The measured LogD of **7** at pH 7.4 was 2.8, which was relatively high in the commonly accepted range of < 3.0 and something we hoped to address in our SAR optimization. In a biophysical confirmation of binding with the KDM5A enzyme via ^{19}F NMR, **7** was found to be competitive with a 17-amino acid histone-derived peptide, in which an additional *p*-CF_3-substituted phenylalanine was added to the C-terminus resulting in the sequence ART-KMe3-QTARKSTGGKAPRKQLA-*p*-CF_3.[8] Given that **7** fulfilled the criteria desired for a structurally and mechanistically distinct hit relative to **6**, we decided to undertake systematic SAR in order to improve its biochemical and cell potency. As the first step toward this goal, a racemic mixture of **7** was subjected to chiral SFC separation to yield a pair of enantiomers which were subsequently profiled. One of the two enantiomers (**9**) was found to be more active than **7**, while maintaining the excellent KDM-selectivity of the original hit. However, even the more active enantiomer **9** was inactive when tested in the cell assay (PC9 H3K4Me3 EC_{50} > 30 μM).

Figure 2.

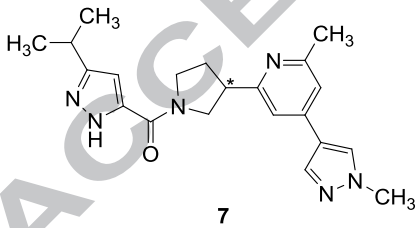

7

Physical properties:

Measured pKa 6.1 (pyridine)	
MW	**378**
LogD	**2.8**
tPSA	**79**
Kinetic solu.	**56 μM**

	7 (racemic)	**8** (enantiomer 1)	**9** (enantiomer 2)
KDM5A IC_{50} [a] (μM)	0.26	0.77	0.16

KDM4C IC_{50}[b] (μM)	>25	ND	13.3
PC9 H3K4Me3[c] EC_{50} (μM)	>30	ND	>30

Figure 2: Structure of the racemic HTS hit **7**, and the biochemical and physical properties. [a] Biochemical assay measuring the demethylation of a H3K4Me3 peptide substrate has been described.[4c] Results shown are the arithmetic mean of at least 3 separate runs. On average, the coefficients of variation were less than 0.10 times the mean for biochemical assay. [b] Biochemical assays for KDM1A, 2B, 3B, 4C, 6A and 7B have been established to assess KDM-selectivity and have been described.[4c] Only the IC_{50} values for KDM4C are shown in this table, since it is closest to KDM5A by sequence and structure. Results shown are the arithmetic mean of at least 3 separate runs. On average, the coefficients of variation were less than 0.21 times the mean for biochemical assay. [c] Cell-based assay measuring the H3K4Me3 level in PC9 cells relative to that of DMSO control has been described.[4c] Results are the arithmetic mean of at least 3 separate runs. On average, the coefficients of variation were less than 0.24 times the mean. ND, not determined.

Despite numerous attempts, we were unsuccessful in obtaining a co-crystal structure of the HTS hit **7** or its more active enantiomer **9** with KDM5A enzyme. Therefore, we relied on docking models to guide our initial SAR optimization. In the docking model of the more active enantiomer **9** with KDM5A enzyme (**Figure 3**), the amide carbonyl was proposed to bind to the active site Fe(II), while the isopropyl-pyrazole *N* was envisioned to have a H-bond interaction with Lys501. Furthermore, two additional H-bond interactions were proposed between **9** and KDM5A: one between Tyr472 and pyridine *N* atom and a second one between Arg73 and the *N*-methyl pyrazole *N* atom.

Figure 3.

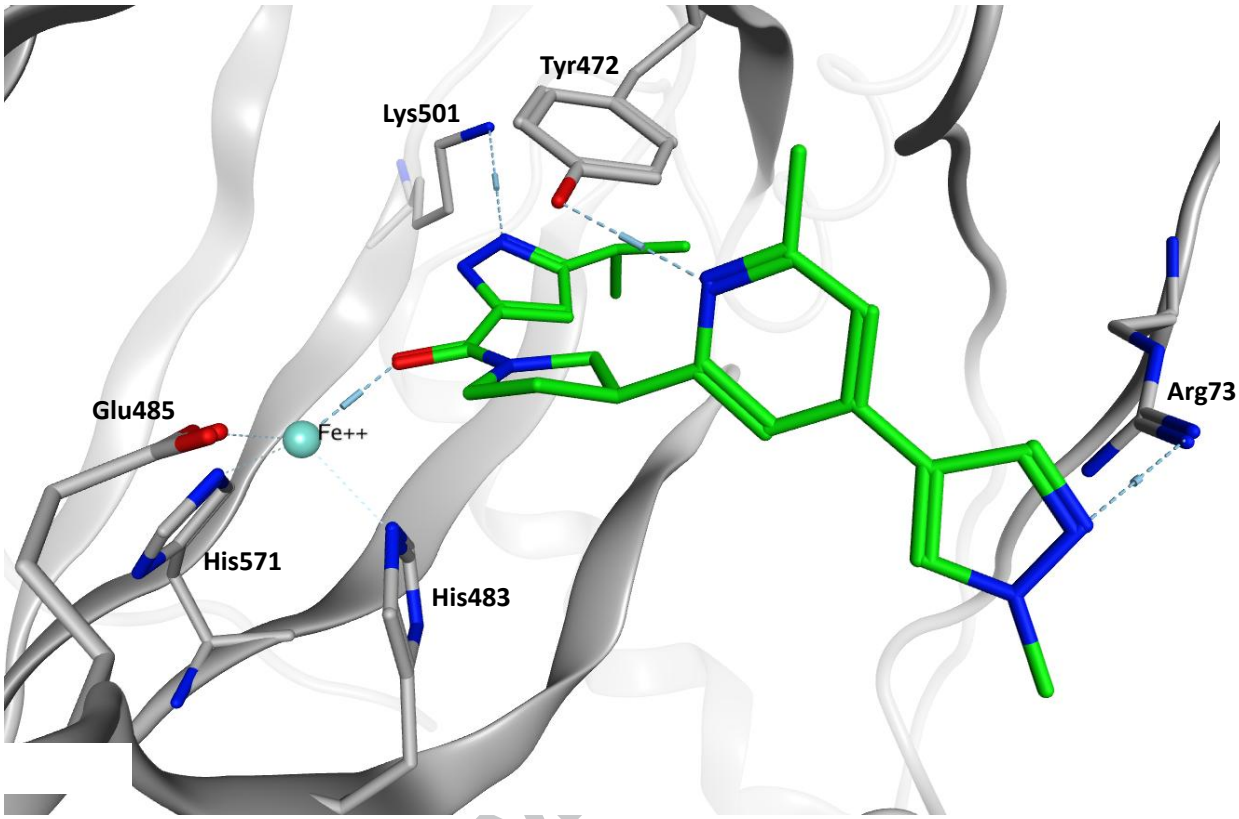

Figure 3: Docking model of **9** in complex with KDM5A enzyme, adopted from a previously published KDM5A structure (PDB code 5CEH).

Even though the binding mode of **9** with KDM5A seemed reasonable, we sought to confirm the binding hypothesis through SAR. Initially we focused on the pyrrolidine amide which was proposed to play a key role in binding to KDM5A via coordination with the active site Fe(II) (**Table 1**). First, we wanted to simplify the stereochemistry of **7** by introducing an olefin in the pyrrolidine ring. This exercise led to analog **10** which was inactive. Replacement of the amide bond in **7** either by a methylene (**11**) or a sulfonamide (**12**) also led to complete loss of potency. Additionally, the pyrrolidine moiety appeared to be critical for activity as both C4- or C3-substituted piperidines (**13** or **14)** were not tolerated. Accordingly, we decided to vary other areas of **7** for optimization.

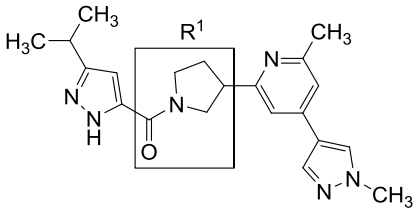

Table 1. SAR for analogs containing pyrrolidine amide modifications

Example*	R^1	KDM5A $IC_{50}{}^{a}$ (nM)
7	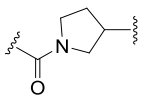	260
10	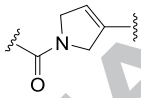	>25000
11	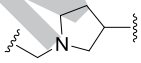	>25000
12	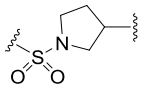	>25000
13	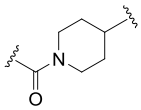	>25000
14	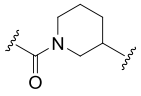	>25000

*Unless specified, a racemic mixture was used for testing. [a] Biochemical assay. Results shown are the arithmetic mean of at least 3 separate runs. On average, the coefficients of variation were less than 0.10 times the mean for biochemical assay.

We next shifted SAR studies to the isopropyl-pyrazole. The associated SAR is summarized in **Table 2**. Complete loss of enzyme potency was noted when the isopropyl-

pyrazole in **7** was replaced with other 5-membered heterocyles (examples **15-17**), despite the fact that a heteroatom (*N* or *O*) was maintained at a location which could maintain a H-bond interaction with Lys501 as proposed in our docking model (Figure 3). We were also somewhat surprised to find that the two *N*-methyl pyrazole regio-isomers **18** and **19** were completely inactive. Additionally, replacement of isopropyl group with *N,N*-dimethylamino moiety (**20**), mimicking the dimethylated lysine substrate, also resulted in >10-fold loss in biochemical potency relative to **7**. To confirm that the isopropyl substituent on the pyrazole was optimal, we systematically examined other alkyl groups at this position (examples **21-25**). Linear or branched alkyls were determined to be less potent than the isopropyl. When a polar functional group was introduced at this position in the form of a methyl ketone (**26**), complete loss of potency was observed. This result suggested that polar substituents were not tolerated in this area.

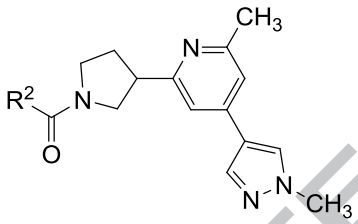

Table 2. SAR for analogs containing modification at the left-hand amide.

Example*	R^2	KDM5A $IC_{50}{}^{a}$ (nM)
7	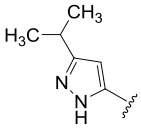	260
15	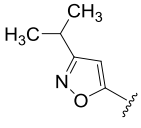	>25000

16	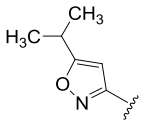	>25000
17	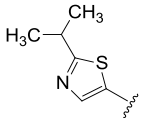	>25000
18	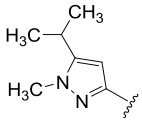	>25000
19	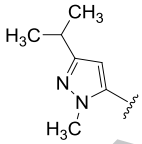	>25000
20	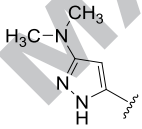	3300
21	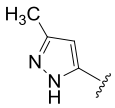	2600
22	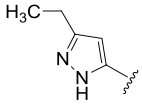	878
23	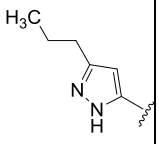	458
24	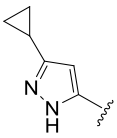	357

25	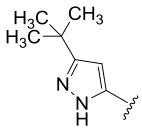	897
26	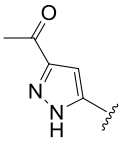	>25000

*Unless specified, a racemic mixture was used for testing. [a] Biochemical assay. Results shown are the arithmetic mean of at least 3 separate runs. On average, the coefficients of variation were less than 0.10 times the mean for biochemical assay.

Subsequently, we explored SAR of the right hand pyrido-methyl-pyrazole moiety (**Table 3**). We initially prepared analog **27** which contained a phenyl group instead of the pyridine moiety present in **7**. However, analog **27** was found to be biochemically inactive suggesting the pyridine *N* atom was critical for binding with KDM5A. Benzyl-substituted pyrazole and other 5- or 6-membered aromatic groups (**28-32**) were tolerated with comparable potency as *N*-methyl pyrazole **7**. Interestingly, 3-methyl phenyl analog (**31**) was tolerated, suggesting the proposed H-bond with Arg73 was not important or our proposed binding model might be incorrect for this area. With an eye towards improving lipophilic ligand efficiency (LLE), we also designed small and polar groups in the form of amides (examples **33** and **34**), in an attempt to replace the methyl-pyrazole moiety. However, neither of these modifications was tolerated. The methyl-pyrazole moiety appeared to have limited impact on potency, with benzyl pyrazole (**28**) and a couple of related analogs (**31** and **32**) only slightly more potent than **7**, albeit at the cost of significantly greater MW and lipophilicity than **7**.

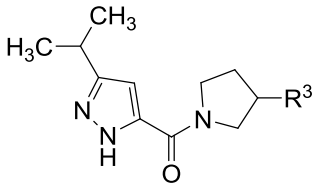

Table 3. SAR for analogs varying the methyl-pyrazole group

Example*	R^3	KDM5A IC_{50} [a] (nM)
7	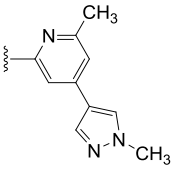	260
27	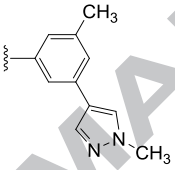	>25000
28	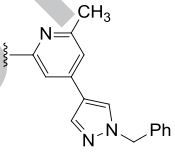	105
29	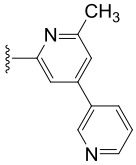	469
30	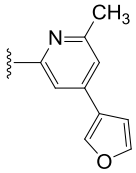	265
31	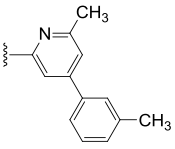	122

32	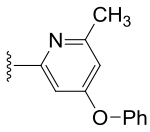	128
33	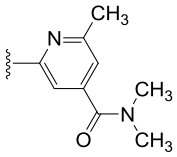	7200
34	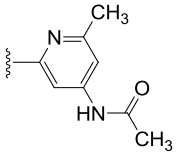	1500

*Unless specified, a racemic mixture was used for testing. [a] Biochemical assay. Results shown are the arithmetic mean of at least 3 separate runs. On average, the coefficients of variation were less than 0.10 times the mean for biochemical assay.

In light of the unproductive SAR outlined above, we made more drastic changes to **7**, particularly with goal towards structural simplification. A significant hurdle associated with the synthesis of **7** and its analogs was the formation of the C-C bond between pyrolidine and pyridine. As a result, we sought to replace the synthetically more challenging C-C bond with a C-X bond in which X could be a heteroatom such as *N* or *O*. We envisioned S_N2 displacement, Buchwald coupling, or amide coupling reactions would access these types of modifications. While unclear such changes would be tolerated by the KDM5A enzyme, we reasoned that the ease of synthesis would allow us to rapidly evaluate the new designs. The resulting SAR is summarized in **Table 4**.

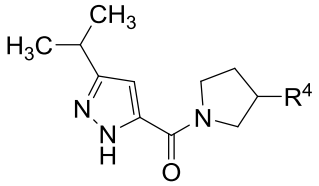

Table 4. SAR for analogs varying the methyl-pyrazole pyridine moiety

Example*	R^4	KDM5A IC_{50} [a] (nM)
7	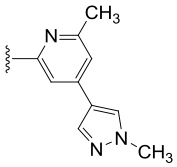	260
35	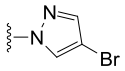	727
36	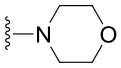	>25000
37	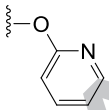	14300
38	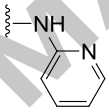	8900
39	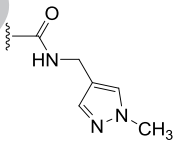	14600
40	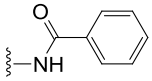	99

*Unless specified, a racemic mixture was used for testing. [a] Biochemical assay. Results shown are the arithmetic mean of at least 3 separate runs. On average, the coefficients of variation were less than 0.10 times the mean for biochemical assay.

We began by replacing the pyridine present in **7** with 3-Br pyrazole (**35**), with the pyrazole *N*2 mimicking the pyridine *N* atom. This change was tolerated, with only 2-3 fold loss in potency. However, saturated heterocycles, exemplified by morpholine (**36**), were completely inactive. We also examined 2-*O*- and 2-*NH*-pyridine derivatives (examples **37-38**) and found that

both changes led to significant loss of potency. Similarly, we synthesized amide analogs, assuming that the carbonyl *O* might fulfill the same role as the pyridine *N* atom in **7**. Unfortunately, methyl-pyrazole amide **39** was not active, while the "reverse amide" **40** showed improved potency against KDM5A relative to **7**.

We obtained a co-crystal structure of the compound **35** in complex with KDM5A at 3.0 Å resolution (**Figure 4**). Despite the fact that a racemic mixture was used in the co-crystallization with KDM5A, one enantiomer with *R*-configuration at C3-position on the pyrrolidine bound in the KDM5A active site. In this structure, Ni^{2+} was used as a catalytically inactive surrogate for Fe^{2+}. Contrary to our initial docking model, the crystal structure showed that the isopropyl-pyrazole and amide were co-planar with the *N1* and carbonyl *O* atoms both coordinated to the metal. In addition, the *N2* atom of the isopropyl-pyrazole was positioned 2.5 Å away from Glu485, suggesting a strong H-bond between the two atoms. These observations suggested that the isopropyl-pyrazole bound to KDM5A in the tautomer depicted in **Figure 4**, in order to achieve two highly favorable interactions with the protein. Thus, the orientation of the compound in the actual binding site was approximately 180° rotated from the docking model. At the opposite end of the inhibitor, the Br-pyrazole *N1'* atom was positioned 2.5 Å away from the sidechain of Lys501, suggesting another potential, though long, H-bond interaction that could be further optimized by replacing the Br-pyrazole ring.

While the majority of compound **35** would overlap the binding pocket of the co-substrate 2-OG, and thus expected to be 2-OG competitive, superposition of the KMe3 histone tail peptide complex from a co-crystal structure of KDM6A (PDB code 3AVR)[9] demonstrated that the isopropyl group occupied the same region of the binding pocket as the trimethylated lysine (**Supplementary Figure S1b**). The crystal structure was consistent with the competition of **7** against histone-derived peptide with binding to KDM5A as determined by ^{19}F NMR described

earlier. This suggested that the pyrolidine amide inhibitors competed with histone peptides for binding with KDM5A, a novel mechanism that has not been reported for KDM5 inhibitors.

Figure 4.

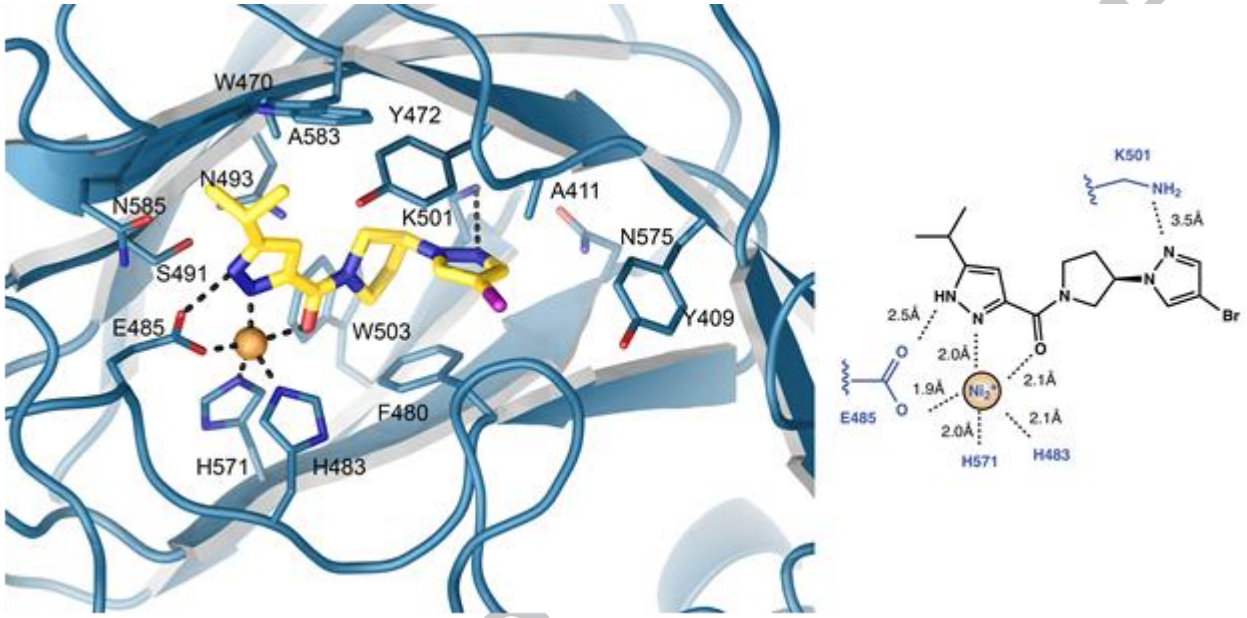

Figure 4. X-ray crystal structure of **35** in complex with KDM5A enzyme. In this crystal structure, Ni^{2+} was used as a catalytically inactive surrogate for Fe^{2+}. The resolution of the X-ray structure is 3.0 Å (PDB code 5V9P). Hydrogen bonds are indicated as dashed lines, and the active site metal ion (Ni^{2+}) is shown as a tan sphere.

With the understanding the true binding mode of the series, we continued SAR explorations of benzamide **40** by preparing and testing a small library of different amides. Representative examples are shown in **Table 5**. Starting with acetyl amide (**41**), a significant drop of potency was observed, compared to benzamide **40**. Ethyl (**42**) and isopropyl amide (**43**) were 3-4-fold more potent than the acetyl amide (**41**). However, no significant improvement was observed with *tert*-butyl amide (**44**). We also evaluated cyclic alkyl amides and were gratified to note that cyclobutyl (**45**) and cyclopropyl amide (**48**) showed the improved biochemical potency

(KDM5A IC_{50} = 80 and 65 nM, respectively). Therefore, we proceeded to separate the two enantiomers of each racemic mixture. One of the cyclobutyl enantiomers (**47**) was more active than the other (**48**) by approximately 3-fold. Similarly, we found that for the cyclopropyl amide pairs (**49** and **50**), one was more potent than the other (45 vs. 90 nM). The more active enantiomer (**50**) also showed cell EC_{50} of 960 nM, meeting the cell potency criteria for an *in vivo* probe. Additionally, as a result of its improved biochemical potency, lower MW and reduced lipophilicity (measured LogD = 1.3 at pH 7.4), **50** showed improved LE (0.49 vs. 0.33) and LLE (5.9 vs. 4.0) when compared to that of the HTS hit **7**.

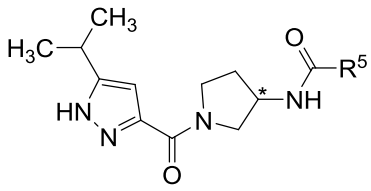

Table 5. SAR of different amides.

Example*	R^5	KDM5A IC_{50}[a] (nM)	PC9 H3K4Me3 EC_{50}[b] (nM)
40	Ph	99	6500
41	Me	1100	ND
42	Et	251	ND
43	*i*Pr	204	ND
44	*t*Bu	198	ND
45	*c*Bu	80	ND
46	*c*Bu (enantiomer 1)	180	ND
47	*c*Bu (enantiomer 2)	60	1500
48	*c*Pr	65	1600

49	*c*Pr (enantiomer 1)	90	ND
50	*c*Pr (enantiomer 2)	45	960

*Unless specified, a racemic mixture was used for testing. [a] Biochemical assay. Results shown are the arithmetic mean of at least 3 separate runs. On average, the coefficients of variation were less than 0.10 times the mean for biochemical assay. [b] Cell-based assay measuring the H3K4Me3 level in PC9 cells relative to that of DMSO control. Results are the arithmetic mean of at least 3 separate runs. On average, the coefficients of variation were less than 0.24 times the mean. ND, not determined.

Subsequently, we obtained a crystal structure of **50** bound to KDM5A at 2.7 Å resolution which helped us define the absolute stereochemistry of the more active enantiomer as *R*-configuration at the C3-position on the pyrrolidine. As shown in **Figure 5**, the overall binding mode of **50** was quite similar to that observed with pyrazole **35**, particularly at the active site in which Ni^{2+} resided. As in the previous structure, the isopropyl-pyrazole was co-planar with the amide carbonyl, resulting in bidentate coordination to the Ni^{2+}, while maintaining the H-bond interaction between the NH and Glu485 of KDM5A.

Figure 5.

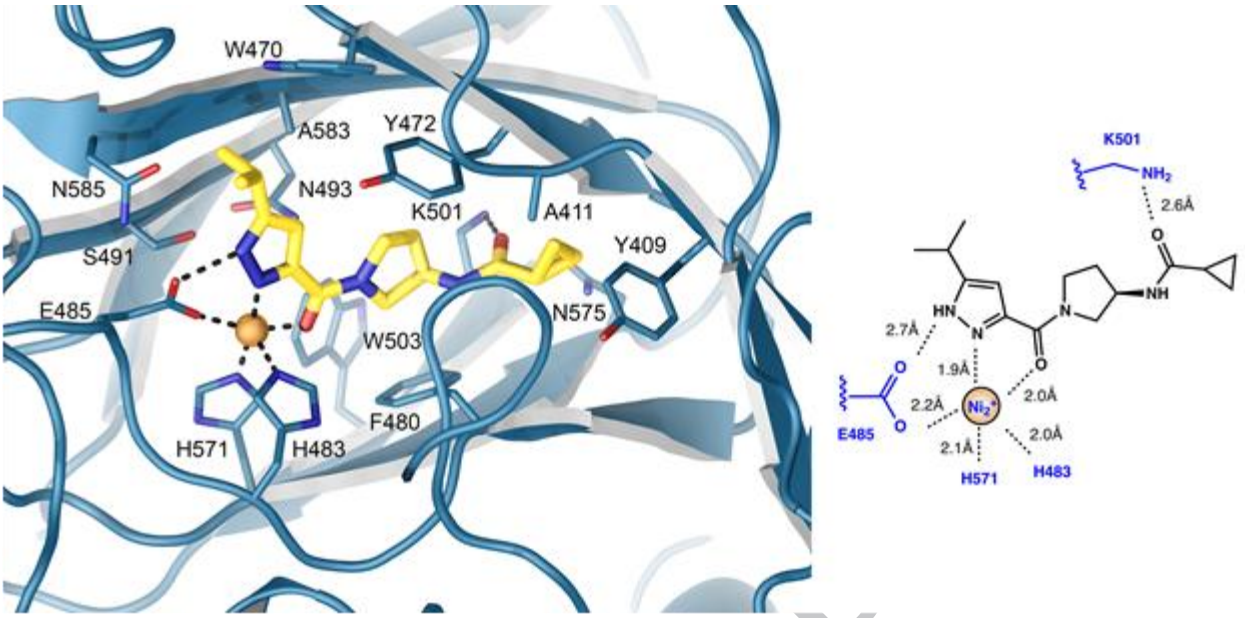

Figure 5. X-ray crystal structure of **50** in complex with KDM5A enzyme. In this crystal structure, Ni^{2+} (tan sphere) was used as a catalytically inactive surrogate for Fe^{2+}. The resolution of the X-ray structure is 2.7 Å (PDB code 5V9T).

While optimizing the biochemical and cell potencies of the pyrolidine amide analogs, we also monitored their metabolic stability both *in vitro* and *in vivo* (mice) in order to identify a potential *in vivo* chemical probe. Those data are summarized in **Table 6**. The more active enantiomer (**9**) of the HTS hit **7** exhibited moderate to high in vitro metabolic instability, as measured with human, rat, and mouse liver microsomes (LM) and hepatocytes (Hep). Consistent with the *in vitro* metabolic stability data in mouse, **9** showed high clearance (CLp 99.9 mL/min/kg) when dosed in mice. MetID studies of **9** with human LM showed the main metabolites formed were due to *N*-demethylation of the methyl pyrazole and oxidation of the methyl group on the pyridine moiety. Consistent with the metID results, replacement of *N*-methylpyrazole-pyridine with cyclopropyl amide (**50**) led to significant improvement in *in vitro* metabolic stability across species. When tested *in vivo*, **50** showed moderate clearance (28

mL/min/kg) in mice with good oral bioavailability (F% 34). Given that **50** showed remarkably low plasma protein binding in mice (40%), the unbound C_{max} observed for the compound following a 5 mg/kg oral dose was ~2x of its cell EC_{50} (960 nM).

Table 6. *In vitro* metabolic stability and *in vivo* PK parameters for select analogs

Example	PPB[a] Human, rat, mouse (%)			In vitro metab. stability						In vivo metab. stability			
				[b]Human, rat, mouse LM (mL/min/kg)			[c]Human, rat, mouse Hepatocyte (mL/min/kg)			[d]Mouse			
										CL_p (mL/min/kg)	$t_{1/2}$ (hr)	V_d (L/kg)	F%
9	95.5	97.3	95.7	7	37	69	12	39	66	99.9	0.3	2.1	94
50	44.0	37.6	40.0	4.2	13	12	1.2	6.3	0.6	28	0.4	0.7	34

[a] Plasma protein binding. [b] Hepatic clearance predicted from liver microsomes. [c] Hepatic clearance predicted from hepatocytes. [d] Female CD-1 mice were given an intravenous dose of 1 mg/kg in PEG/EtOH/H_2O as a solution and an oral dose of 5 mg/kg in MCT as a suspension.

Based on this cell potency and *in vivo* PK profile, **50** met our *in vivo* tool compound criteria and was selected for additional profiling. Compound **50** was shown to be a pan-KDM5 enzyme inhibitor, with IC_{50} of 56 and 55 nM against KDM5B and KDM5C isoforms, respectively. However, it was significantly less potent against other KDM enzymes (1A, 2B, 3B, 4C, 6A, 7B), inhibiting KDM4C the strongest with an IC_{50} of 4.1 μM. Thus **50** displayed 91-fold selectivity for KDM4C vs. KDM5A. When tested at 10 μM in Invitrogen kinase (300 kinases) and Cerep (40 enzymes/receptors/ion channels) panels, **50** did not show > 50% inhibition against any target.

In conclusion, we were attracted to a novel HTS hit **7** as a structurally distinct scaffold, with different mechanism of KDM5A inhibition relative to the molecules we had previously

disclosed. After comprehensive SAR studies that were guided by structural biology, we were able to identify a biochemically and cellular more potent compound **50**, with promising *in vivo* PK profiles. Remarkably, we significantly reduced MW and lipophilicity (LogD) for the top lead (**50**) of this scaffold from the original hit (**7**). As a result, **50** was selected from the second scaffold for *in vivo* biological studies, results from which will be disclosed in the future.

ACKNOWLEDGEMENT

We thank, Mengling Wong, Michael Hayes, Baiwei Lin, Yutao Jiang, and Yanzhou Liu for purification and analytical support; Daniel Hascall, Grady Howes, Gigi Yuen, and Garima Porwal for compound management support; Leslie Wang, Hoa Le and Qin Yue for ADME support; Emile Plise and Jonathan Cheng for MDCK data; Ning Liu for microsomal stability; Jasleen Sodhi for reversible CYP inhibition measurement; Quynh Ho for plasma protein binding measurement. We thank the BME group at Genentech for insect cell expression. We thank the staff at LS-CAT at the APS and Shamrock Inc for data collection. This research used resources of the Advanced Photon Source, a U.S. Department of Energy (DOE) Office of Science User Facility operated for the DOE Office of Science by Argonne National Laboratory under Contract No. DE-AC02-06CH11357. Use of the LS-CAT Sector 21 was supported by the Michigan Economic Development Corporation and the Michigan Technology Tri-Corridor (Grant 085P1000817). We also thank the staff at beamline 5.0.2 at ALS. This research used resources of the Advanced Light Source, which is a DOE Office of Science User Facility under contract no. DE-AC02-05CH11231.

A. SUPPLEMENTARY DATA

Supplementary data associated with this article can be found, in the online version, at http://xxx.

REFERENCES

1. (a) Margueron, R.; Reinberg, D. *Nat. Rev. Genet.* **2010**, *11*, 285. (b) Itoh, Y.; Suzuki, Miyata, N. *Mol. BioSyst.* **2013**, *9*, 873. (c) Black, J. C.; Van Rechem, C.; Whetstine, J. R. *Mol. Cell* **2012**, *48*, 491. (d) Greer, E. L.; Shi, Y. *Nat. Rev. Genet.* **2012**, *13*, 343. (e) Lohse, B.; Kristensen, J. L.; Kristensen, L. H.; Agger, K.; Helin, K.; Gajhede, M.; Clausen, R. P. *Bioorg. Med. Chem.* **2011**, *19*, 3625. (f) Suzuki, T.; Miyata, N. *J. Med. Chem*. **2011**, *54,* 8236.

2. (a) Marks, P. A.; Rifkind, R. A.; Richon, V. M.; Breslow, R.; Miller, T.; Kelly, W. K. *Nature Rev. Cancer* **2001**, *1*, 195; (b) Manal, M.; Chandrasekar, M. J. N.; Priya, J.; Nanjan, M. J. *Bioorg. Chem*. **2016**, *67*, 18.

3. (a) Kooistra, S. M.; Helin, K. *Nat. Rev. Mol. Cell Biol.* **2012**, *13*, 297. (b) Højfeldt, J. W.; Agger, K.; Helin, K. *Nat. Rev. Drug Discov.* **2013**, *12*, 917.

4. (a) Sharma, S. V.; Lee, D. Y.; Li, B.; Quinlan, M. P.; Takahashi,F.; Maheswaran, S.; McDermott, U.; Azizian, N.; Zou, L.; Fischbach, M. A.; Wong, K.; Brandstetter, K.; Wittner, B.; Ramaswamy, S.; Classon, M.; Settleman, J. *Cell* **2010,** *141*, 69. (b) Roesch, A.; Vultur, A.; Bogeski, I.; Wang, H.; Zimmermann, K. M.; Speicher, D.; Körbel, C.; Laschke, M. W.; Gimotty, P. A.; Philipp, S. E.; Krause, E.; Pätzold, S.; Villanueva, J.; Krepler, C.; Fukunaga-Kalabis, M.; Hoth, M.; Bastian, B. C.; Vogt, T.; Herlyn, M. *Cancer Cell* **2013**, *23*, 811. (c) Vinogradova, M.; Gehling, V. S.; Gustafson, A.; Arora, S.; Tindell, C. A.; Wilson, C.; Williamson, K. E.; Gangurde, P.; Manieri, W.; Busby, J.; Flynn, M.; Lan, F.; Kim, H.-J.; Odate, S.; Cochran, A. G.; Liu, Y.; Wongchenko, M.; Yang, Y.; Cheung, T.; Maile, T. M.; Lau, T.; Costa, M.; Hegde, G.

V.; Jackson, E.; Pitti, R.; Arnott, A..; Bailey, C.; Bellon, S.; Cummings, R. T.; Albrecht, B. K.; Harmange, J. C.; Kiefer, J. R.; Trojer, P.; Classon, M. *Nat. Chem. & Biol.*, **2016**, *12*, 531.

5. (a) Cloos, P. A. C.; Christensen, J.; Agger, K.; Mailica, A.; Rappsilber, J.; Antal, T.; Hansen, K. H.; Helin, K. *Nature* **2006**, *442*, 307. (b) McAllister, T. E.; England, K. S.; Hopkinson, R. J.; Brennan, P. E.; Kawamura, A.; Schfield, C. J. *J. Med Chem*. **2016**, *59*, 1308. (c) Westaway, S. M.; Preston, A. G. S.; Baker, M. D.; Brown, F.; Brown, J. A.; Campbell, M.; Chung, C.; Diallo, H.; Douault, C.; Drewes, G.; Eagle, R.; Gordon, L.; Haslam, C.; Hayhow, T. G.; Humphreys, P. G.; Joberty, G.; Katso, R.; Kruidnenier, L.; Leveridge, M.; Liddle, J.; Mosley, J.; Muelbaier, M.; Randle, R.; Rioja, I.; Rueger, A.; Seal, G. A.; Sheppard, R. J.; Singh, O.; Taylor, J.; Thomas, P.; Thomson, D.; Wilson, D. M.; Lee, K.; Prinjha, R. K. *J Med. Chem*. **2016**, *59*, 1357. (d) Westaway, S. M.; Preston, A. G. S.; Barker, M. D.; Brown, F.; Brown, J. A.; Campbell, M.; Chung, C.; Drewes, G.; Eagle, R.; Garton, N.; Gordon, L.; Haslam, C.; Hayhow, T. G.; Humphreys, P. G.; Joberty, G.; Katso, R.; Kruidnenier, L.; Leveridge, M.; Pemberton, M.; Seal, G. A.; Shipley, T.; Singh, O.; Suckling, C. J.; Taylor, J.; Thomas, P.; Wilson, D. M.; Lee, K.; Prinjha, R. K. *J Med. Chem*. **2016**, *59*, 1370. (e) Bavetsias, V.; Lanigan, R. M.; Ruda, G. F.; Atrash, B.; McLaughlin, M. G.; Tumber, A.; Mok, N. Y.; Le Bihan, Y.-V.; Dempster, S.; Boxall, T. J.; Jeganathan, F.; Hatch, S. B.; Savitsky, P.; Velupillai, S.; Krojer, T.; England, K. S.; Sejberg, J.; Thai, C.; Donovan, A.; Pal, A.; Scozzafava, G.; Bennett, J. M.; Kawamura, A.; Johnsson, C.; Szykowska, A.; Gileadi, C.; Burgess-Brown, N. A.; Delft, F.; Oppermann, U.; Walters, Z.; Shipley, J.; Raynaud, F. I.; Westaway, S. M.; Prinjha, R. K.; Fedorov, O.; Burke, R.; Schofield, C. J.; Westwood, I. M.; Bountra, C.; Muller, S.; Montfort, R. L. M.; Brennan, P. E.; Blagg, J. *J Med. Chem*. **2016**, *59*, 1388. (f) Johansson, C.; Velupillai, S.; Tumber, A.; Szykowska, A.; Hookway, E. S.; Nowak, R. P.; Strain-Damerell, C.; Gileadi, C.; Phipott, M.; Burgess-Brown, N.; Wu, N.; Nuzzi, A.; Steuber, H.; Egner, U.; Badock, V.; Munro, S.;

LaThangue, N. B.; Westaway, S.; Brown, J.; Athanasou, N.; Prinjha, R.; Brennan, P. E.; Oppermann, U. *Nat. Chem. & Biol.*, 2016, 12, 539. (g) Horton, J. R.; Liu, X.; Gale, M.; Wu, L.; Shanks, J. R.; Zhang, X.; Webber, P. J.; Bell, J. S. K.; Kales, S. C.; Mott, B. T.; Rai, G.; Jansen, D. J.; Henderson, M. J.; Urban, D. J.; Hall, M. D.; Simeonov, A.; Maloney, D. J.; Johns, M. A.; Fu H.; Jadhav, A.; Vertino, P. M.; Yan, Q.; Cheng, X. *Cell Chem. Biol*. **2016**, *23*, 769. (h) Labadie, S.; Dragovich, P. S.; Ackerman, L.; Cummings, R.; Deshmukh, G.; Gustafson, A.; Harmange, J. C.; Kiefer, J. R.; Liang, J.; Liederer, B. M.; Liu Y.; Manieri, W.; Mao, W.; Murray, L.; Ortwine, D. F.; Trojer, P.; VanderPorten, E.; Vinogradova, M. *Bioorg. Med. Chem Lett*. **2016**, *26*, 4492. (i) Gehling, V. S.; Bellon, S.; Harmange, J. C.; Leblanc, Y.; Odate, S.; Buker, S.; Lan F.; Sandy, P.; Bergeron, L.; Mao, W.; Gustafon, A.; Liu Y.; VanderPorten, E.; Trojer, P.; Albrecht, B. K. *Bioorg. Med. Chem Lett.*, **2016**, *26*, 4350. (j) Tumber, A.; Nuzzi, A.; Hookway, E. S.; Hatch, S. B.; Velupillai, S.; Johansson, C.; Kawamura, A.; Savitsky, P.; Yapp, C.; Szykowska, A.; Wu, N.; Bountra, C.; Strain-Damerell, C.; Burgess-Brown, N. A.; Ruda, G. F.; Fedorov, O.; Munro, S.; England, K. S.; Nowak, R. P., Schofield, C. J.; La Thangue, N. B.; Pawlyn, C.; Davies, F.; Morgan, G.; Athanasou, N.; Muller, S.; Oppermann, U.; Brennan, P. E. Cell Chem. Biol. http://dx.doi.org/10.1016/j.chembiol.2017.02.006.

6. Liang, J.; Zhang, B.; Labadie, S. Ortwine, D. F.; Vinogradova, M.; Kiefer, J. R.; Gehling, V. S.; Hamange, J.-C.; Cummings, R.; Lai, T.; Liao, J.; Zheng, X.; Liu, Y.; Gustafson, A.; Van der Porten, E.; Mao, W.; Liederer, B. M.; Deshmukh, G.; Classon, M.; Trojer, P.; Dragovich, P. S.; Murray, L. *Bioorg. Med. Chem Lett*. **2016**, *26*, 4036.

7. (a) Hopkins, A. L.; Groom, C. R.; Alex A. *Drug Discov. Today* **2004**, *9*, 430. (b) Leeson, P. D.; Springthorpe, B. *Nature Rev. Drug Discov*. **2007**, *6*, 881.

8. Dalvit, C.; Papeo, G.; Mongelli, N.; Giordano, P.; Saccardo, B.; Costa, A.; Veronesi, M.; Ko, S-Y. *Drug Develop. Res.* **2005**, *64*, 105.

9. Sengoku, T.; Yokoyama, S. Gene & Develop. **2011**, *25*, 2266.